Highly enhanced electrochemical performance of silicon-free platinum–yttria stabilized zirconia interfaces

Joshua L. Hertz · Avner Rothschild · Harry L. Tuller

Abstract In the drive to achieve economically viable solid oxide fuel cells, efforts have been directed towards substantially decreasing their operating temperature. Unfortunately, these efforts have been hindered by extremely sluggish electrode kinetics at reduced temperatures. In this report, we show that silicon impurities on the surface of the electrolyte play a critical role in influencing electrode kinetics. More specifically, improvements by as much as three orders of magnitude are reported for the performance of platinum electrodes on yttria-stabilized zirconia electrolytes prepared as high purity thin films with a largely Si-free surface. These improvements in performance are estimated to enable operation of a solid oxide fuel cell down to approximately 400 °C.

Keywords Yttria-stabilized zirconia (YSZ) · Platinum · Polarization resistance · Impedance spectroscopy · Solid oxide fuel cells (SOFC)

J. L. Hertz (✉) · A. Rothschild · H. L. Tuller
Department of Materials Science and Engineering,
Massachusetts Institute of Technology,
77 Massachusetts Avenue,
Cambridge, MA 02139, USA
e-mail: joshua.hertz@nist.gov

Present address:
J. L. Hertz
National Institute of Standards and Technology,
100 Bureau Drive, MS8362,
Gaithersburg, MD 20899, USA

Present address:
A. Rothschild
Department of Materials Engineering,
Technion—Israel Institute of Technology,
Technion City,
Haifa 32000, Israel

1 Introduction

While solid oxide fuel cell (SOFC) power sources offer the potential for broad fuel flexibility and efficient chemical to electrical energy conversion, they suffer from high operating temperatures (typically 800–1000 °C) [1, 2]. These temperatures are required to achieve sufficiently high ionic conductivity in the solid electrolyte, typically yttria-stabilized zirconia (YSZ), and adequate electrode kinetics to ensure efficient cell operation. High operating temperatures, however, significantly increase system and operation costs and lead to reduced operating life. They are especially problematic for micro-SOFCs, which offer great promise as portable power sources [3–6]. Highly conductive and/or thin film electrolytes have demonstrated low ohmic resistance at reduced operating temperatures (500–700 °C), putting the burden of performance largely on the electrochemical kinetics at the electrodes [7]. In particular, the oxygen reduction reaction (ORR) at the air/cathode/electrolyte interface is believed to be the main limitation in reducing the operating temperatures of SOFCs [8, 9].

The ORR at the air/cathode/YSZ interface:

$$\tfrac{1}{2}\,O_2(gas) + 2\,e^-(cathode) \rightarrow O^{2-}(YSZ) \qquad (1)$$
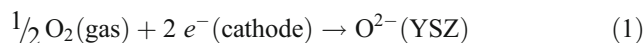
involves O_2 molecules in the gas phase, electrons in the cathode, and oxygen ions (O^{2-}) in the YSZ electrolyte [10]. The reaction is believed to occur, largely, in the close vicinity of the common gas/cathode/electrolyte contact (called the triple phase boundary or TPB), and to proceed in a multistep series of sub-reactions [10]. Unfortunately, despite many years of research, a detailed understanding of electrode performance remains lacking [8]. This is due, in large part, to the complex microstructures and chemistries achieved at the electrolyte-electrode interface following the

powder processing and high-temperature sintering routes typically used to create these devices [11].

It is known from a number of studies that YSZ surfaces are commonly coated with impurities that have segregated to the surface during high temperature processing [12, 13]. Impurity segregation to surfaces and grain boundaries is a general phenomenon associated with high temperature ceramic processing and has been shown, in particular, to lead to the degradation of the electrical and mechanical properties of YSZ [14–16]. To what degree these impurities affect the reaction kinetics of electrodes on YSZ surfaces, however, remains unclear [8]. Only a few studies have examined, in some detail, the possible role of impurities in the oxygen exchange process at the surfaces of SOFC electrodes [17–20]. De Ridder et al. [18] found that a monolayer of impurities, including Si, Na, and Ca, reduced oxygen exchange at the cathode surface. Hansen et al. [19] found that while anodes of both impure (99.8% Ni) and pure nickel (99.995% Ni) resulted in the formation of impurity ridges in the vicinity of the triple-phase boundary, generally speaking the pure Ni led to much lower electrode impedances. These limited studies suggest that impurities, emanating either from the electrolyte or the electrode, tend to degrade electrode performance. To date, however, no system has been sufficiently free of various impurities to be able to make a clear connection between a given impurity and its impact on electrode performance.

In the present study, photolithographically-defined, dense, thin film platinum microelectrodes are used to systematically study the effect of YSZ electrolyte surface purity on electrode performance while maintaining a well-defined and fixed sample geometry. Unlike porous electrodes in conventional SOFC designs, such microelectrodes enable systematic investigations of electrochemical processes at the TPB, as demonstrated for a number of materials systems [21–26]. In this study, platinum was used as a model system because it is a classic, well-studied electrode with simple chemistry and low oxygen diffusivity

such that oxygen incorporation is confined to the TPB at the electrode perimeter [10, 25, 27–30]. In addition, Pt is of interest as a micro-SOFC electrode component because it is an excellent catalyst for redox reactions, is stable in both oxidizing and reducing environments, and—for the amount used per micro-device—not likely to be a challenging cost issue [5]. Identical Pt electrodes were formed on the surfaces of traditionally processed tape-cast polycrystalline, polished single crystal and thin film YSZ. The yttria dopant concentration of the bulk samples was nominally 8 mol% while for the films it was roughly 4.5 mol%. Somewhat better performance was found for films with this lower Y concentration; this effect will be explored in future publications. As we demonstrate, Si impurities at the YSZ surface appear to have a drastic effect on electrode performance.

2 Experimentation

Polished YSZ single crystal wafers (Coating and Crystal Technology) with both (100) and (111) orientation were used as substrates. One hundred nanometer thick YSZ films were sputter deposited onto the substrates from a Y_9Zr_{91} metal alloy target as described elsewhere [31]. Films were deposited with the substrate unheated or held at 600 °C using a halogen lamp mounted behind the substrate. The "unheated" substrates were subject to some latent heating (~130 °C) due to ion bombardment during sputtering. As seen in Fig. 1, the unheated films had grains that varied in size from 10–40 nm in diameter while the films deposited at 600 °C had features of ~30 nm as determined by atomic force microscopy. For comparison, additional samples were made without the YSZ thin films, placing the electrodes directly upon the YSZ single crystals as well as upon polycrystalline, tape cast YSZ.

Dense platinum electrodes, 150 nm thick, were then deposited on the surface of the YSZ films as well as on

Fig. 1 Atomic force microscope topographic images of YSZ films deposited on an (a) unheated and (b) 600 °C single crystal YSZ substrate. Total lateral range is 1 μm in both directions. Brightness of the pixel indicates the height, with the total range from black to white given in each image as "Z scale." The two bright white features in (b) are believed to be dust or other flaws
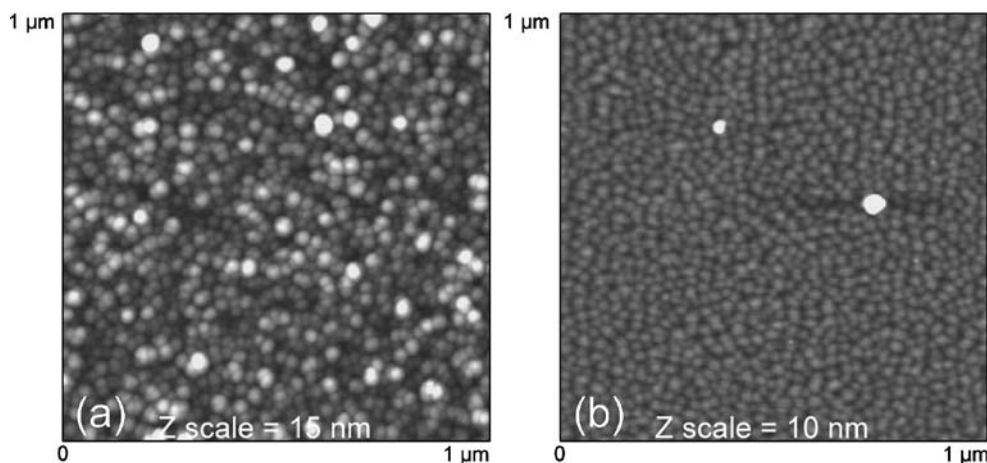
bulk single crystal and polycrystalline YSZ specimens by DC sputtering from a >99.99% pure platinum target (Birmingham Metal, Co.) at a plasma power of 50 W in a working pressure of 5 mTorr of argon. A standard "lift-off" photolithographic technique was used to pattern these films into interdigitated electrodes [31]. A sample schematic is shown in Fig. 2(a). Figure 2(b) shows the sub-micron edge definition of a platinum electrode patterned on the surface of a YSZ film. By digitally tracing the edge, the lateral waviness was estimated to have added about 10% to the intended TPB lengths (i.e., the nominal perimeter).

The polarization resistances of symmetric two-electrode Pt|YSZ|Pt configurations were measured using electrochemical impedance spectroscopy (Solartron 1260 impedance analyzer operated between 1 mHz and 10 MHz at an oscillating voltage of 20 mV) in an open-air probe station (Karl Suss model SOM4) fitted with a hot stage (Linkam Scientific Instruments model TS1500) at temperatures between 150 and 450 °C. A typical impedance spectrum is shown in Fig. 3(a). Data files were fitted to an equivalent circuit (shown in Fig. 3(b)) using Scribner Associate's ZView software.

Based on the magnitudes and activation energies of the derived resistances and capacitances, the impedance features were assigned physical meaning. The constant phase elements (CPEs) were pseudo-capacitive and accounted for non-ideal capacitive behavior. Inductor L1, which combined with the other elements to produce the offset from the origin, was due to the cables and leads and had a value of ~4 μH for all of the spectra collected. The high frequency semicircle, labeled 'I' in the figure and modeled with circuit components R2 and CPE2, is ascribed to the electrolyte impedance. The low frequency semicircle, labeled 'II' and modeled with circuit components R4 and CPE4, is ascribed to the electrochemical processes at the electrodes [10, 27–32]. A third, minor feature, which overlaps the high frequency side of arc 'II' but is not immediately apparent in the figure, is believed to be due to current constriction near the TPB [33]. The current constriction, modeled with

circuit components R3 and CPE3, may also change with impurity concentration; however, this effect was difficult to determine in these samples and, in any case, is not likely to be important to the performance of any practical electrode. In this article, we focus on semicircle 'II'.

X-ray photoelectron spectroscopy (XPS) measurements were carried out (Kratos Analytical model Axis Ultra) to examine the surface chemistry. Binding energy values were calibrated by setting the peak energy of the carbon 1 s emission to 285.0 eV. Spectra were measured at take-off angles relative to the surface normal of 0°, 35°, and 70°. Larger angles are more surface sensitive, with the analyzed sample depth roughly estimated at 10 nm at 0° and 2 nm at 70°. Spectra were analyzed using Casa Software's CasaXPS software, version 2.3.13Dev9.

3 Results and discussion

The electrode conductances, normalized by the TPB lengths, are plotted in an Arrhenius fashion in Fig. 4. The values for the electrodes on the tape-cast YSZ surface are the lowest. Electrode conductance values for Pt on the 600 °C-deposited YSZ film and on the single crystal YSZ surfaces range from a factor of two to ten times higher than that on the tape-cast YSZ. These values are similar to the best reported values obtained with sputtered [25, 34], gauze [34, 35], and wire [36, 37] platinum electrodes on YSZ, though there is significant variability within reported literature values. Note that, despite the simplified electrode structures employed in previous studies, the TPB lengths used to normalize those values are sometimes rather crude estimates. In addition, those values have been extrapolated from measurements typically above 600 °C.

The electrodes on the YSZ films deposited on unheated single crystal YSZ substrates exhibited remarkably higher conductances, nearly three orders of magnitude higher than those of the same Pt electrodes deposited directly onto the single crystal YSZ substrates, suggesting that the

Fig. 2 The interdigitated electrode structures. (a) Schematic diagram of the electrodes, showing the 150 nm thick electrode fingers (*grey*) on the surface of a YSZ electrolyte (*white*). (b) Scanning electron micrograph of the edge of a platinum electrode on a YSZ film, viewed from above. *Bar*= 2 μm
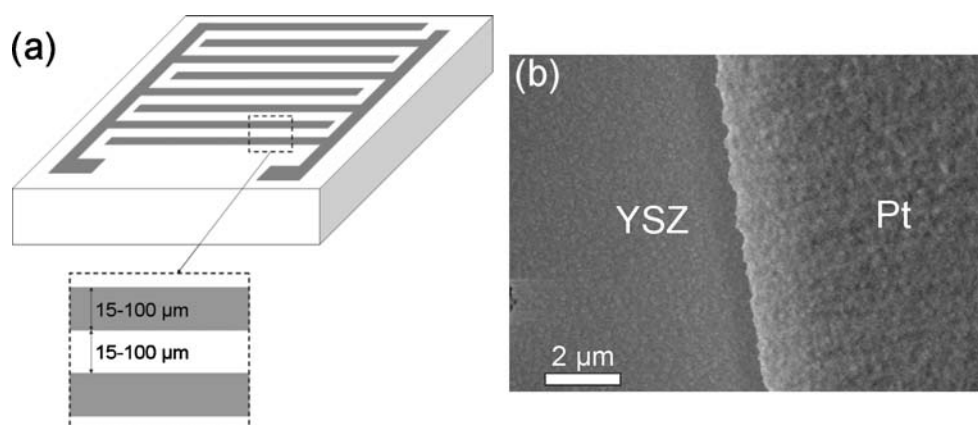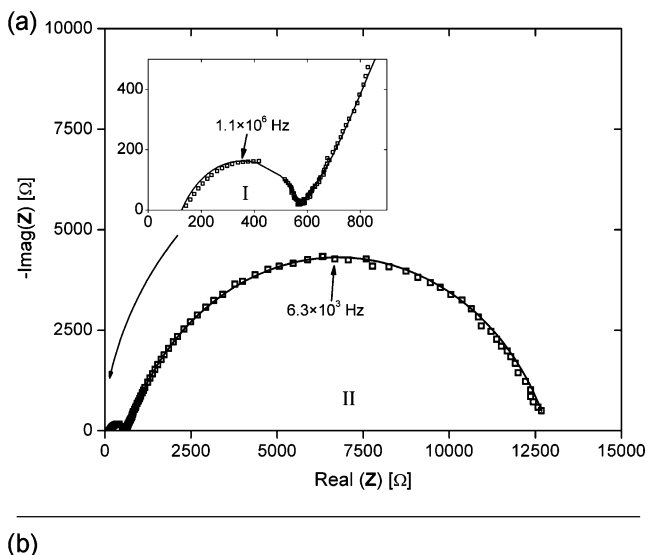
Fig. 3 (a) A typical impedance spectrum, measured at 302° C; from a YSZ single crystal sample with a YSZ film sputtered onto the unheated surface and with electrodes of total perimeter length 103 cm, spaced 25 μm apart. *Dots* represent raw data while the *line* represents the best-fit curve from the equivalent circuit model. The *inset* magnifies the low impedance portion of the spectrum, which exhibits features due to the ohmic resistance of the electrolyte. The 'missing' data points in the *inset* were from a frequency region where the instruments were measured to be out of calibration. Not shown is the data collected at highest frequencies, which extended below the real axis into the inductive region of the impedance plane. (b) Equivalent circuit used to fit the impedance spectra. See text for a detailed explanation of the circuit model

binding energy peaks at around 529.9 eV (labeled O1s(I) in the figure) and 532.5 eV (labeled O1s(II) in the figure), similar to those found here, have been correlated to O bonded to Zr and Si, respectively [38]. A strong peak at 532.5, as is the case in the Si contaminated YSZ surfaces, points to a high percentage of inactive oxygen strongly bonded to Si.

Previous measurements of platinum electrodes on YSZ, have either been performed at high temperatures (>900 °C) or with specimens that had seen similar temperatures during high-temperature ceramic processing. As discussed, these temperatures are conducive to silicon contamination of the YSZ surfaces by segregation of impurities from the bulk in addition to migration of impurities from the furnace walls. It is our belief that previous measurements have been on impure surfaces, thereby degrading the measured electrode kinetics of the YSZ interface. De Ridder et al. [18] estimated that bulk impurity concentrations would have to be reduced to below 10 ppm—from typical raw materials levels of 100–1,000 ppm [39]—to prevent significant impurity segregation to the surfaces of traditionally processed YSZ. The thin film YSZ specimens prepared here are unique in that they are prepared from high purity metal alloy targets (nominal Si concentration of 3.6 ppm). The
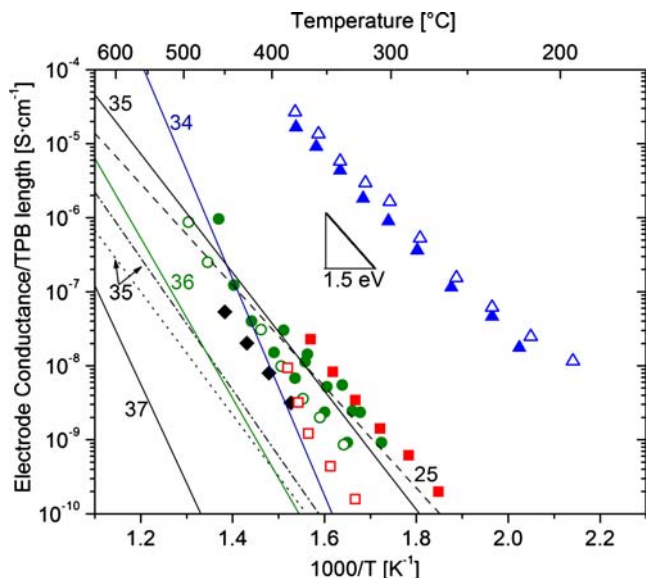
performance of traditionally processed electrolytes can be enhanced by coating their surface with a low-temperature deposited thin film electrolyte. It is interesting to note that all of the samples measured had relatively similar area-normalized electrode capacitances of around 50 μF·cm^{-2}, which tended to increase slightly with increasing temperature.

In order to trace the origin of the very large changes in electrochemical performance to the electrolyte surface chemistry, these results were compared to the XPS results. Figure 5 shows that there is significant silicon contamination on the surfaces of the tape-cast specimen, single crystal specimen, and the single crystal with 600 °C deposited film specimen, but little such contamination on the surface of the single crystal coated with the unheated film. The angle resolved measurements show that when silicon contamination occurs, it is preferentially located on the outermost atomic monolayer(s).

A change in oxygen bonding is the most likely means for the electrolyte surface to play a role in the electrode activation polarization. Figure 5 confirms that the silicon contamination is commensurate with such a change. Oxygen

Fig. 4 The low frequency (electrode polarization) conductance normalized by the TPB length for the tape-cast YSZ (*closed diamonds*), untreated single crystal (*closed circles*, *open circles*), single crystal with 100 nm of a 600 °C-deposited YSZ film (*closed squares*, *open squares*), and single crystal with 100 nm of an unheated deposited YSZ film (*closed triangles*, *open triangles*). *Closed symbols* represent (100)-oriented YSZ single crystal substrates while *open symbols* represent (111)-oriented single crystal substrates. The *lines* are extrapolations from the indicated references (note, [36] and [37] are based on measurements in pure O$_2$ whereas all other measurements were in air). A reference line indicates a slope of 1.5 eV. Values from samples with TPB lengths ranging from about 25–170 cm are presented

Fig. 5 X-ray photoelectron spectra for the (**a**) tape-cast YSZ, (**b**) single crystal YSZ and (**c**) 600°C-deposited film show, in addition to the expected Y doublet peak, contamination from Si; the spectrum for (**d**) the film deposited without substrate heating, shows little such contamination. Higher energy portions of these spectra (**e**, **f**, **g**, and **h**) show that silicon contamination is commensurate with changes in the oxygen bonding state (labeled 'I' and 'II'). There are three spectra in all of the graphs displayed, corresponding to sample orientations within the XPS of 0° (*top*), 35° (*middle*), and 70° (*bottom*); as the angle is increased, the technique becomes more surface sensitive. Note that the high-angle measurements in (**a**) and (**d**) may have had an anomalous error during collection. Ordinate units are arbitrary
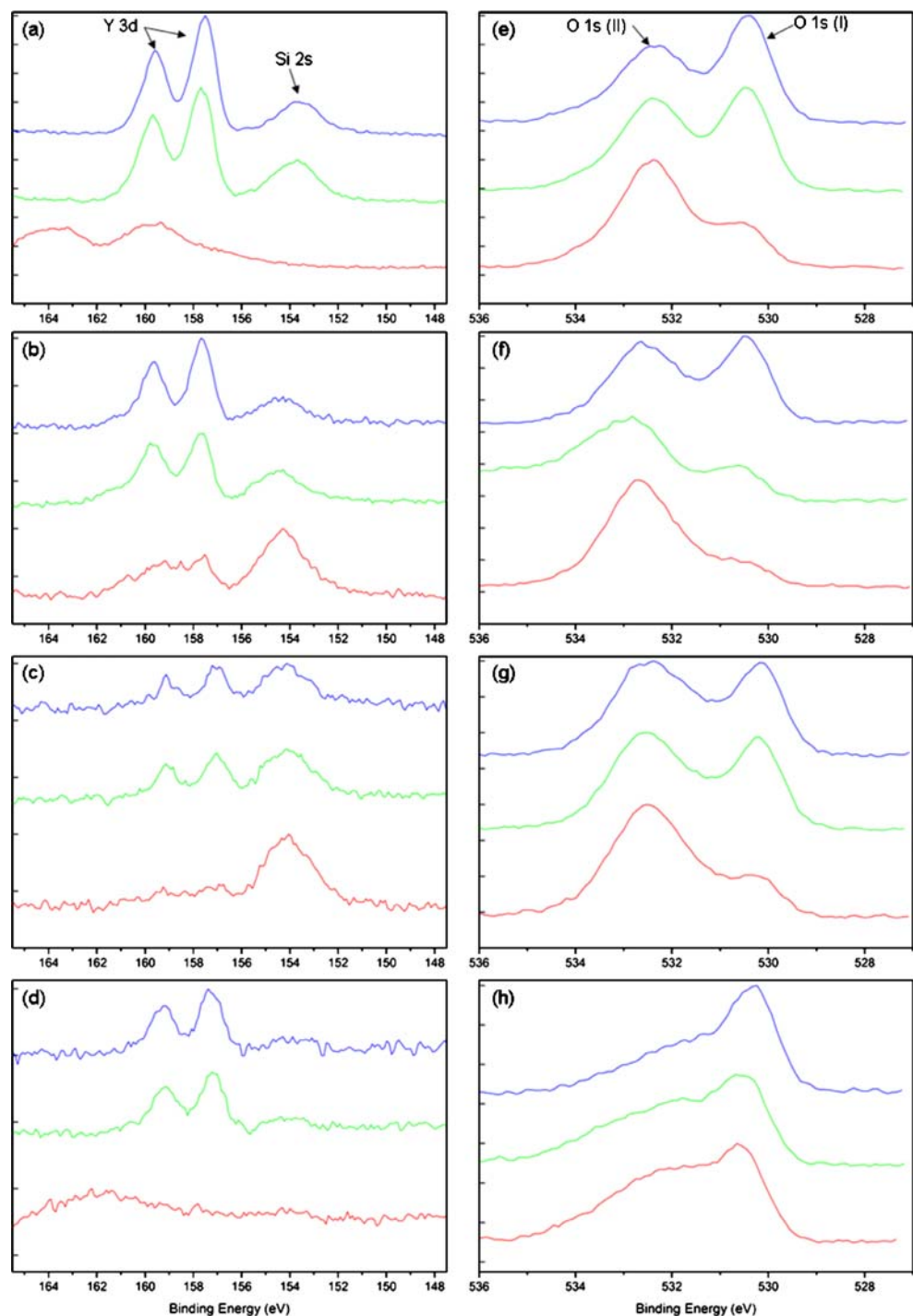
films prepared at low temperatures are thus likely to have much lower Si surface contamination than any other specimens examined to date, as confirmed by our XPS measurements.

Consistent with this interpretation, the performance of the electrodes placed on a (100)-oriented single crystal was found to improve dramatically after etching the sample for 5 min in concentrated hydrofluoric acid. This can be seen in Fig. 6. XPS measurements confirmed that etching removed silicon from the YSZ surface. It should be noted, however, that the surface likely experienced other complex chemical and morphological changes in addition to the removal of the silicon. For example, some amount of etching of the YSZ or Pt surfaces may have occurred. Note that no fluorine was found on the surface during the XPS analysis.

To ensure that the markedly increased low frequency conductance of the low temperature prepared YSZ films was not due to a surface leakage effect, measurements were
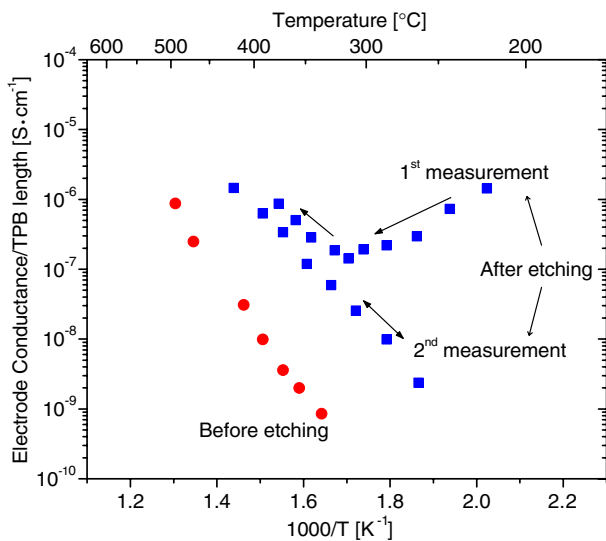
Fig. 6 The low frequency (electrode polarization) conductance, normalized by the TPB length, for platinum electrodes on a single crystal YSZ substrate before (*closed circles*) and after (*closed squares*) etching in concentrated hydrofluoric acid. Transient behavior is found in the unusual measured conductance during the first heating cycle

repeated using a large Pt paste electrode placed on the back surface of the electrolyte (shown schematically in Fig. 7). The effective inter-electrode spacing increased by a factor of about 100 in this measurement, yet the low frequency conductance changed little. Thus, we conclude that this is indeed an electrode polarization resistance and not surface leakage.

Other potential factors related to YSZ processing which could possibly influence electrode performance include the grain boundary density intersecting the surface and the crystallographic orientation. To directly test these possibilities, samples were produced using YSZ films that were deposited on unheated and 600 °C amorphous silica substrates. These films exhibited low-frequency resistances (Fig. 8) and XPS (Fig. 9) results nearly identical to the corresponding films deposited on single crystal YSZ. Since
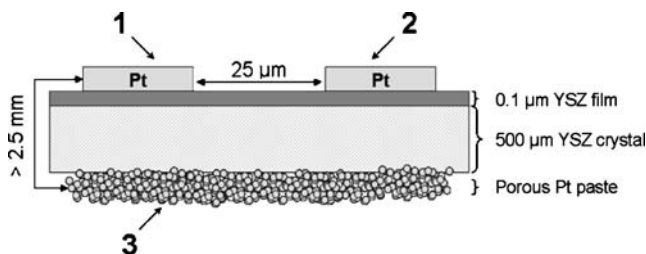

Fig. 7 The measurement setup (not drawn to scale) used to ensure that the low frequency resistance was not related to a spurious leakage current between the sputtered electrodes. Impedance spectra were measured between sputtered platinum electrodes 1 and 2, which were spaced by 25 μm, and between sputtered electrode 1 and platinum paste electrode 3, which were separated along the surface by more than 2.5 mm. The triple phase boundary length of the dense sputtered electrode 1 was much less than that of platinum paste electrode 3, so electrode 1 was the rate limiting electrode for both measurements
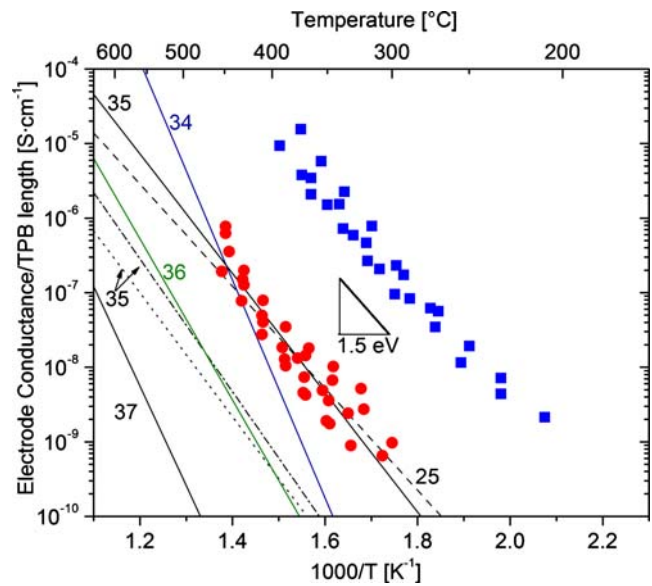

Fig. 8 The low frequency—electrode polarization—conductance, normalized by the TPB length, for platinum electrodes on YSZ films deposited on an unheated (*closed squares*) and 600 °C (*closed circles*) fused silica substrate. The *dashed lines* are extrapolated from the indicated references (note [36] and [37] are based on measurements in pure O_2 whereas all other measurements were in air). A reference line indicates a slope of 1.5 eV. Values from samples with TPB lengths ranging from about 25–170 cm are presented

both of the films deposited on silica were polycrystalline with very small grain sizes (~30 nm) and only slight texture (Fig. 10), neither grain boundary density, nor crystallographic orientation can be the source of the electrochemical performance differences.

The above results demonstrate that a critical limitation of current SOFC technology is likely due to an unexpectedly large effect of silicon impurities in degrading oxygen exchange kinetics at the electrodes. Having shown this, more careful study into the as yet unknown effects of YSZ microstructure and dopant concentration can be undertaken. Specifically, since improved electrode performance was found with films that never experienced high temperatures, the role of nanocrystalline or possibly residual amorphous phase must also be investigated. The fact that the activation energy (~1.5 eV) characterizing the electrode reaction remained nearly fixed for all samples (see Fig. 2) indicates that silicon acts to block active sites supporting oxygen exchange and does not participate directly in the exchange reaction. This is consistent with the blocking action of calcium impurities, as deduced by isotopic exchange experiments [18]. If micro-SOFCs are to be produced on silicon substrates, these results suggest that extreme care must be taken to control chemical interactions and interdiffusion between film and substrate. On the other hand, this work has shown that low temperature, thin film processing routes can be used to create ceramics with sufficient surface purity to avoid these effects. Indeed, this

Fig. 9 X-ray photoelectron spectra for YSZ films deposited on a (**a**) 600 °C and (**b**) unheated fused silica substrate. The film deposited at 600 °C shows, in addition to the expected Y doublet peak, contamination from Si; the film deposited without substrate heating shows little such contamination. Higher energy portions of these spectra (**c**, **d**) show that the silicon contamination is commensurate with changes in the oxygen bonding state (labeled 'I' and 'II'). There are three spectra in all of the graphs displayed, corresponding to sample orientations within the XPS of 0° (*top*), 35° (*middle*), and 70° (*bottom*). As the angle is increased, the technique becomes more surface sensitive. Note that the middle-angle measurements in (**b**) and (**d**) may have had an anomalous error during collection. Ordinate units are arbitrary
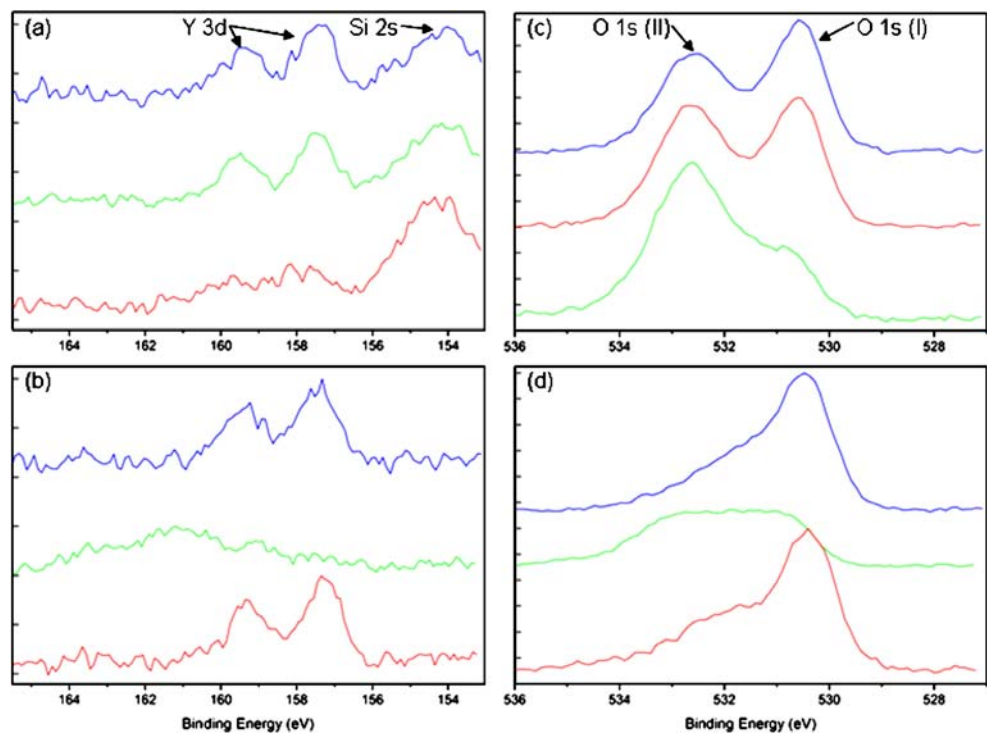
may have been the cause of the surprisingly high performance demonstrated recently in a thin film SOFC [5].

Finally, we consider how the effects discovered here may affect the operation of a micro-solid oxide fuel cell device that uses a platinum cathode. Given the activation energy of roughly 1.5 eV, a decrease in cathode polarization resistance by a factor of 1,000 should allow, all else being equal, a reduction in operating temperature of 150–200 °C. Using the electrode conductance per unit of TPB length as measured on the unheated films in this study, a reasonable

target area specific resistance [4] of 0.5 $\Omega \cdot cm^2$ can be achieved at 400 °C in a single layer, dense Pt cathode using 0.25 μm lithography or its equivalent. Somewhat higher performance cathodes have been demonstrated at these temperatures [40, 41]; however, these were thick, porous materials which convey geometric advantage. Thus, if processing methods with both improved microstructure and impurity-free surfaces can be found, even lower area specific resistances can be expected.
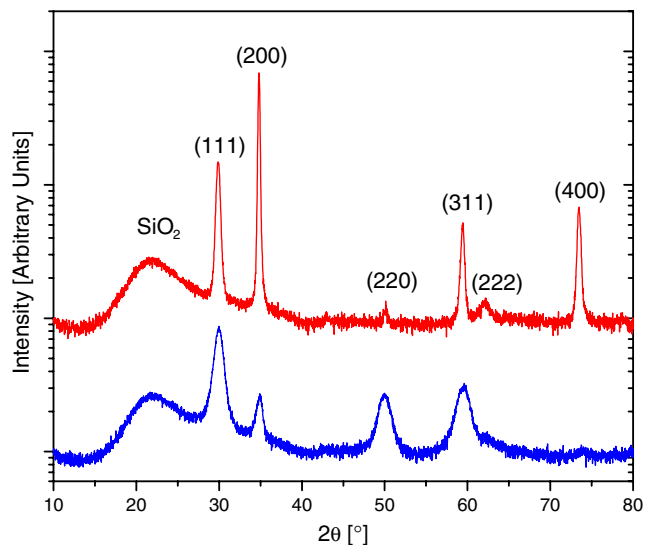
4 Conclusions

Based on the very large change in electrode polarization and the concomitant finding of silicon impurities on the surfaces of the poorer-performing samples, it is believed that impurities play a key role in the sluggish electrode kinetics on YSZ surfaces. Siliceous impurities, which are very often found on YSZ surfaces after high-temperature processing, seem to increase the polarization resistance by blocking the transfer of oxygen between the atmosphere and the electrolyte. One possible solution to this issue is to coat traditionally processed YSZ with high purity YSZ films grown at reduced temperature.

Fig. 10 X-ray diffraction patterns of YSZ films deposited on an unheated (*blue, bottom*) and 600 °C (*red, top*) fused silica substrate. *Numbers in parenthesis* indicate Miller indices of cubic YSZ peak locations. Peak location of the fused silica substrate is also indicated

References

1. N.Q. Minh, J. Am. Ceram. Soc **76**, 563 (1993)
2. S.C. Singhal, K. Kendall, *High temperature solid oxide fuel cells*: *fundamentals*, *design and applications* (Elsevier, Oxford, 2003), pp. 1–19
3. X. Chen, N.J. Wu, L. Smith, A. Ignatiev, Appl. Phys. Lett **84**, 2700 (2004)
4. Z. Shao, S.M. Haile, J. Ahn, P.D. Ronney, Z. Zhan, S.A. Barnett, Nature **435**, 795 (2005)
5. H. Huang, M. Nakamura, P. Su, R. Fasching, Y. Saito, F.B. Prinz, J. Electrochem. Soc **154**, B20 (2007)
6. A. Bieberle-Hütter, D. Beckel, A. Infortuna, U.P. Muecke, J.L.M. Rupp, L.J. Gauckler, S. Rey-Mermet, P. Muralt, N.R. Bieri, N. Hotz, M.J. Stutz, D. Poulikakos, P. Heeb, P. Müller, A. Bernard, R. Gmür, T. Hocker, J. Power Sources **177**, 123 (2008)
7. B.C.H. Steele, A. Heinzel, Nature **414**, 345 (2001)
8. S.B. Adler, Chem. Rev **104**, 4791 (2004)
9. J. Fleig, Annu. Rev. Mater. Res **33**, 361 (2003)
10. J.E. Bauerle, J. Phys. Chem. Solids **5**, 2657 (2006)
11. J.R. Wilson, W. Kobsiriphat, R. Mendoza, H.-Y. Chen, J.M. Hiller, D.J. Miller, K. Thornton, P.W. Voorhees, S.B. Adler, S.A. Barnett, Nature Materials **5**, 541 (2006)
12. A. Bernasik, J. Phys. Chem. Solids ed. by K. Kowalski, A. Sadowski**63**, 233 (2002)
13. M. Backhaus-Ricoult, M.-F. Trichet, Solid State Ionics **150**, 143 (2002)
14. M. Aoki, Y.-M. Chiang, I. Kosacki, L.J.-R. Lee, H. Tuller, Y. Liu, J. Am. Ceram. Soc **79**, 1169 (1996)
15. S.P.S. Badwal, J. Drennan, A.E. Hughes, B.A.A. Sexton, Mater. Sci. Forum **34–36**, 195 (1988)
16. G.M. Ingo, G. Padeletti, Surf. Interface Anal **21**, 450 (1994)
17. J.-M. Bae, B.C.H. Steele, Solid State Ionics **106**, 247 (1998)
18. M. de Ridder, A.G.J. Vervoort, R.G. van Welzenis, H.H. Brongersma, Solid State Ionics **156**, 255 (2003)
19. K.V. Hansen, K. Norman, M. Mogensen, J. Electrochem. Soc **151**, A1436 (2004)
20. J.J. Zhu, J.G. van Ommen, A. Knoester, L. Lefferts, J. Catal **230**, 291 (2005)
21. J. Mizusaki, H. Tagawa, T. Saito, K. Kamitani, T. Yamamura, K. Hirano, S. Ehara, T. Takagi, T. Hikita, M. Ippommatsu, S. Nakagawa, K. Hashimoto, J. Electrochem. Soc **141**, 2129 (1994)
22. A. Bieberle, L.P. Meier, L.J. Gauckler, J. Electrochem. Soc **148**, A646 (2001)
23. V. Brichzin, J. Fleig, H.-U. Habermeier, J. Maier, Electrochem. Solid-State Lett **3**, 403 (2000)
24. R. O'Hayre, F.B. Prinz, J. Electrochem. Soc **151**, A756 (2004)
25. R. Radhakrishnan, A.V. Virkar, S.C. Singhal, J. Electrochem. Soc **152**, A927 (2005)
26. E. Koep, C. Compson, M. Liu, Z. Zhou, Solid State Ionics **176**, 1 (2005)
27. A. Mitterdorfer, L.J. Gauckler, Solid State Ionics **117**, 187 (1999)
28. A. Mitterdorfer, L.J. Gauckler, Solid State Ionics **117**, 203 (1999)
29. M.G.H.M. Hendriks, B.A. Boukamp, J.E. ten Elshof, W.E. van Zyl, H. Verweij, Solid State Ionics **146**, 123 (2002)
30. D. Vladikova, J.A. Kilner, S.J. Skinner, G. Raikova, Z. Stoynov, Electrochim. Acta **51**, 1611 (2006)
31. J.L. Hertz, H.L. Tuller, J. Electroceram **13**, 663 (2004)
32. J.L. Hertz, Ph.D. Thesis, Massachusetts Institute of Technology, Cambridge, MA (2006)
33. J.L. Hertz, H.L. Tuller, Solid State Ionics **178**, 915 (2007)
34. M.J. Verkerk, M.W. Hammink, A.J. Burggraaf, J. Electrochem. Soc **130**, 70 (1983)
35. S.N. Shkerin, Russ. J. Electrochem **39**, 863 (2003)
36. S.N. Shkerin, S. Gormsen, M. Mogensen, Russ. J. Electrochem **40**, 136 (2004)
37. C. Schwandt, W. Weppner, J. Electrochem. Soc **144**, 3728 (1997)
38. S. Damyanova, P. Grange, B. Delmon, J. Catal **168**, 421 (1997)
39. R. Vaßen, N. Czech, W. Malléner, W. Stamm, D. Stöver, Surf. Coat. Tech **141**, 135 (2001)
40. Z. Shao, S.M. Haile, Nature **431**, 170 (2004)
41. C. Xia, M. Liu, Adv. Mater **14**, 521 (2002)